International Journal of Multiphase Flow 35 (2009) 566–579

Contents lists available at ScienceDirect

International Journal of Multiphase Flow

journal homepage: www.elsevier.com/locate/ijmulflow

Flow patterns of *n*-hexadecane–CO_2 liquid–liquid two-phase flow in vertical pipes under high pressure

Ronghong Lin, Lawrence L. Tavlarides *

Department of Biomedical and Chemical Engineering, Syracuse University, 121 Link Hall, Syracuse, NY 13244, United States

ARTICLE INFO

Article history:
Received 12 August 2008
Received in revised form 30 January 2009
Accepted 10 February 2009
Available online 26 February 2009

Keywords:
Liquid–liquid two-phase flow
Flow pattern
Hexadecane–carbon dioxide system
High pressure

ABSTRACT

To promote a better understanding of liquid–liquid two-phase flow behavior, particularly under high pressure, flow patterns of *n*-hexadecane–CO_2 liquid–liquid two-phase upward flow in vertical stainless steel pipes were experimentally investigated. Observations were made in two 0.0015 m I.D. pipes of different lengths (0.068 m and 0.5 m) under high pressure varying from 10.3 to 29.6 MPa using a high pressure visualization system. The total flow rate was fixed at 2.0×10^{-6} m^3/min, while the flow rate ratio (φ) varied from 0.05 to 19. Bubbly flow, plug flow, slug flow, annular flow, and near-one-phase flow regions were found in both pipes, while stratified flow was observed only in the 0.068 m pipe. Flow pattern maps were constructed in the flow rate ratio versus pressure graph, which demonstrates significant impacts of flow rate ratio, pipe length, and pressure on flow patterns. These impacts are discussed in detail. To the authors' best knowledge, this work is the first attempt to observe complex liquid–liquid two-phase flow behavior with flow pattern transitions under high pressure, and contributes to a better understanding of liquid–liquid two-phase flow behavior.

1. Introduction

The steadily increasing consumption of energy due to the blooming global economy brings significant environmental impacts. The adverse health and climatic effects of combustion byproducts have led to considerable emission regulations. Thus the controlling emissions, while maintaining high energy efficiency, becomes a big challenge for both academia and industry. Aiming to reduce harmful emissions, increase diesel engine efficiency, and enhance diesel engine performance, a great number of investigations focusing on almost every aspect of diesel fuel combustion process have been carried out. Recently, Tavlarides and Anitescu (2006) proposed a new concept to improve diesel engine combustion by using supercritical fuel combustion technology. A similar concept to improve fuel injection by dissolving exhaust gas into diesel oil was reported by Merkisz et al. (2007). These processes involve complex multiphase flow phenomena. Thus, a better understanding of liquid–liquid two-phase flow and its transition to the supercritical phase is important to facilitate this concept.

Flow of a mixture of two immiscible liquids is also encountered in many other industrial processes, such as the petroleum industry where oil and water are often produced and transported together (Jana et al., 2006a), the pharmaceutical industry where tubular reactors of small diameter are sometimes used for continuous production (Wegmann and von Rohr, 2006), and the fine chemical industry where microreactors have been used to intensify mass transfer limited reactions (Burns and Ramshaw, 2001; Kashid and Agar, 2007). Optimal design of such facilities relies on substantial knowledge of the flow inside a pipe. Although investigations of liquid–liquid two-phase flow started in the middle of the last century, this field had been quite inactive until the middle of the 1990s when the interest of liquid–liquid two-phase flow was revived due to its importance in the petroleum industry (Hewitt, 1997). Since then, a great number of investigations of liquid–liquid two-phase flow have been conducted over a wide range of experimental conditions and a variety of flow patterns of liquid–liquid two-phase flow have been reported. Table 1 summarizes experimental investigations of oil–water two-phase flow patterns since 1996.

Liquid–liquid two-phase flow in pipes of small diameters (or microchannels) has recently received increasing attention. Burns and Ramshaw (2001) developed a multiphase microreactor by using slug flow in a narrow channel to enhance interfacial mass transfer and the reaction rate. Tokeshi et al. (2002) investigated liquid–liquid two-phase flow on a microchip which was designed based on a combination of microunit operations and a multiphase flow network to minimize sample analysis time. Zhao et al. (2006) studied immiscible liquid–liquid two-phase flow behavior in T-junction rectangular microchannels. Kashid and Agar (2007) investigated flow regimes, slug size, and pressure drop in the cyclohexane–water two-phase flow in a transparent poly(tetrafluoroethylene) (PTFE) capillary with a Y-junction mixing element.

* Corresponding author. Tel.: +1 315 443 1883; fax: +1 315 443 9175.
E-mail addresses: rlin01@syr.edu (R. Lin), lltavlar@syr.edu (L.L. Tavlarides).

0301-9322/$ - see front matter © 2009 Elsevier Ltd. All rights reserved.
doi:10.1016/j.ijmultiphaseflow.2009.02.008

Table 1
Summary of experimental systems of oil–water two-phase flow.

Authors	Pipe inclination (flow direction)	Fluids	Pipe material	Diameter (m)	Length (m)	Superficial velocity, m/s (flow rate, $\times 10^{-6}$ m^3/min)		Temp. (°C)	Flow pattern map available
Farrar and Bruun (1996)	Vertical (upward)	Kerosene, water	Acrylic resin	0.078	1.5	N/A		N/A	No
Nädler and Mewes (1997)	Horizontal	Oil, water	Perspex	0.059	48	Mixture	0.1–1.6	10–30	Yes
Beretta et al. (1997a)	Horizontal	Oil, water	Glass	0.003	1	Oil Water	(5.4–55.8) (up to 564)	15–25	Yes
Trallero et al. (1997)	Horizontal	Oil, water	Acrylic resin	0.05013	15.54	N/A		N/A	Yes
Beretta et al. (1997b)	Horizontal	Oil, water	Glass	0.003	1	N/A		15–25	No
Angeli and Hewitt (1998)	Horizontal	Oil, water	Stainless steel Perspex	0.0243 0.024	9.7 9.5	Mixture	0.3–3.9	20	No
Angeli and Hewitt (2000)	Horizontal	Oil, water	Stainless steel Perspex	0.0243 0.024	9.7 9.5	Mixture	0.2–3.9	20	Yes
Fairuzov et al. (2000)	Horizontal	Crude oil, water	N/A	0.3635	N/A	N/A		N/A	Yes
Shi et al., 2001	Horizontal	Oil, water	N/A	0.1	18	Mixture	0.4–3	25	No
Raj et al. (2005)	Horizontal	Kerosene, water	Acrylic resin	0.0254	2.13	Kerosene Water	0.03–1.6 0.03–1.6	N/A	No
Ioannou et al. (2005)	Horizontal	Oil, water	Stainless steel Acrylic resin	0.06 0.032	16.6	Mixture	3.5–5 4–7 small pipe	N/A	No
Jana et al. (2006a)	Vertical (upward)	Kerosene, water	Acrylic resin	0.0254	1.4	Kerosene Water	0.05–1.5 0.05–1.5	30	Yes
Chakrabarti et al. (2006)	Horizontal	Kerosene, water	Perspex	0.025	3	N/A		N/A	Yes
Wegmann and von Rohr (2006)	Horizontal	Paraffin oil water	Glass	0.0056 0.007	5	Mixture	Max. 4.5	~20	Yes
Rodriguez and Bannwart (2006)	Vertical (upward)	Oil, water	Glass	0.0284	2.5	N/A		Room Temp.	Yes
Abduvayt et al. (2006)	Horizontal, Inclined, Vertical	Oil, water	N/A	0.1064	120	N/A		35	Yes
Lum et al. (2006)	Inclined (upward and downward)	Oil, water	Stainless steel	0.038	8x2	Mixture	0.7–2.5	N/A	Yes
Rodriguez and Oliemans (2006)	Horizontal, Inclined	Oil, water	Steel perspex	0.0828	15	N/A		N/A	Yes
Piela et al. (2006)	Horizontal	Oil, water	Acrylic resin	0.016	6×2 4.5×2	Oil Water	1.35–3.5 1–3	N/A	No
Zhao et al. (2006)	Vertical (upward)	Oil, water	Acrylic resin	0.04	3.8	Oil Water	0.024–0.198 0.12–0.89	N/A	Yes
Hu et al. (2007)	Vertical (upward and downward)	Oil, water	Stainless steel	0.038	3.2 2.3	N/A		N/A	No
Kashid and Agar (2007)	Horizontal	Cyclohexane water	PTFE capillary	0.00025–0.001	N/A	Cyclohexane Water	(0.84–3.36) (0.84–3.36)	N/A	Yes
Mandal et al. (2007)	Horizontal	Oil, water	PMMA	0.025 0.012	2	Oil Water	0.03–1.5 0.03–1.5	N/A	Yes

Flow patterns observed and reported for liquid–liquid two-phase flow in vertical pipes can be generally classified into four main types: (1) dispersed flow with fine droplets of one liquid in the other, (2) bubbly flow with large droplets of one liquid in the other, (3) intermittent flow with one fluid in the other, which can be further divided into plug flow and slug flow, and (4) annular flow where one fluid forms the core while the other forms the annulus. In each type of flow patterns, different forms exist and have been reported and discussed in the literature. Sketches of flow patterns of liquid–liquid two-phase flow in vertical pipes are given in Fig. 1. A comprehensive summary of flow patterns and their transitions can be found elsewhere (Brauner, 2004).

It is generally understood that flow patterns are influenced by a variety of factors, which can be categorized into three groups: (1) fluid properties (e.g. density, viscosity, surface or interface tension, mutual solubility, etc.), (2) channel properties (e.g. geometry, size, and orientation), and (3) operation conditions (e.g. temperature, pressure, flow directions, flow rates, and flow rate ratios). A large number of investigations have been carried out to address these impacts. Angeli and Hewitt (1998) investigated the effect of wall material on flow patterns, leading to a conclusion that pressure gradients in two-phase pipe flow can be greatly affected by wall material due to the difference in both wall roughness and the wettability characteristics. Similar results were reported by Ioannou et al. (2005). Angeli and Hewitt (2000) also observed that the tendency for dispersion was greatly increased in the stainless steel pipe, while oil tended to be the continuous phase for a wider range of flow conditions in the acrylic pipe than in the stainless steel pipe.

Mandal et al. (2007) investigated the influence of pipe size on the flow patterns by conducting experiments in two parallel PMMA test rigs of diameter 0.012 m and 0.025 m. Different flow patterns were observed in the two test rigs under the same flow conditions, which verified the impact of pipe size on flow pattern. It was also found that entrance conditions appeared to affect flow distribution in the downstream, implying that flow pattern may be changed significantly by introducing two fluids in a different way.

The impact of pipe orientation on flow pattern is so remarkable that most experiments were focused on one orientation, horizontal, vertical, or in lesser cases, inclined. Different flow patterns have

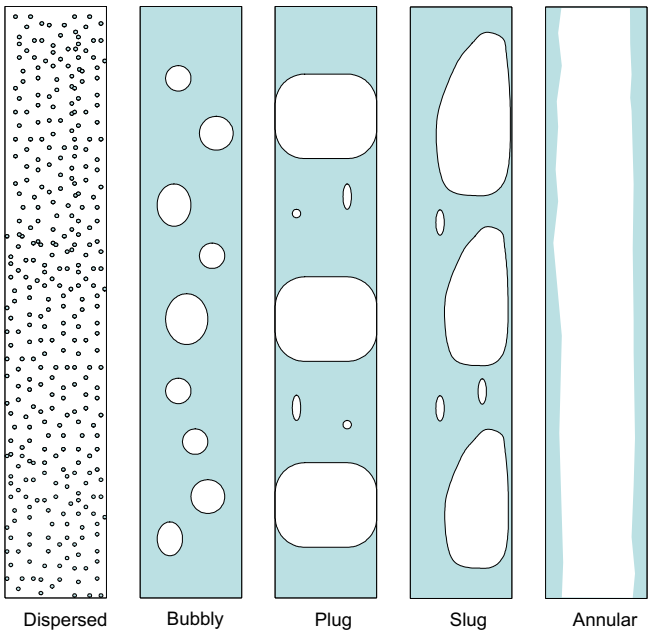

Fig. 1. Flow patterns of liquid–liquid two-phase vertical upward flow in pipes.

been recognized and plotted in separated flow pattern maps for different orientations. Lum et al. (2006) experimentally investigated the effect of upward (+5° and +10°) and downward (−5°) inclination on oil–water flow pattern. It was found that stratified flow became wavier as the degree of inclination increased from the horizontal and it completely disappeared in the downward flow. Similar results were reported by Rodriguez and Oliemans (2006).

Along with two-phase flow pattern studies, a variety of flow pattern detection techniques have been developed and applied to laboratory scale investigations, among which, the direct visual observation method, photographic techniques (Chen et al., 1988; Wong and Yau, 1997; Lin et al., 1999; Lin and Kew, 2001; Pawloski et al., 2004; Satitchaicharoen and Wongwises, 2004; Hwang et al., 2005; Liu et al., 2005; Wongwises and Pipathattakul, 2006), conductance probes (Jana et al., 2006a; Hernández et al., 2006), impedance probes (Seleghim and Hervieu, 1998; Angeli and Hewitt, 2000), hot-film anemometry (Farrar and Bruun, 1996), and optical probes (Celata et al., 1991; Hamad et al., 1997, 2000; Jana et al., 2006b, 2007; Chakrabarti et al., 2007) have widely been used. Such techniques are capable to identify flow patterns by measuring a physical or thermodynamic property that is different for two phases such as density, concentration, conductivity, capacitive, heat capacity, and optical properties. It is worth pointing out, however, that almost all probe techniques are intrusive and need to be immersed into the flow field, which more or less interrupts two-phase structures. Thus, care should be taken when selecting probe techniques for flow pattern detections and other two-phase flow measurements. A literature survey (Lin, 2008) on flow pattern detection techniques shows that the photographic technique mentioned above has mostly been used in liquid–liquid two-phase flow pattern investigations due to its low cost and easy operation.

Although a substantial amount of work has been done to explore the nature of liquid–liquid two-phase flow, impacts of fluid properties, channel properties, and operation conditions on liquid–liquid two-phase flow patterns are not well understood. The goal of this study is to promote a better understanding of flow patterns of liquid–liquid two-phase pipe flow, particularly, flow patterns encountered in supercritical fuel delivery systems. *n*-Hexadecane (*n*-HD) was selected as a surrogate of diesel fuel. Experiments were conducted for *n*-HD–CO_2 liquid–liquid two-phase upward flow in vertical stainless steel pipes of 0.0015 m inner diameter (I.D.). The photographic technique accompanied by a high-pressure view cell was used for flow pattern observation. Impacts of flow rate ratio, pipe length, and pressure on flow patterns are discussed.

2. Experiments

2.1. Materials

Liquid CO_2 and *n*-HD used in this study were supplied by Airgas, Inc. and Sigma–Aldrich, Inc., respectively. Thermodynamic and transport properties of the materials considered in this work include density, viscosity, interfacial tension, and solubility. Densities and viscosities of liquid CO_2 and *n*-HD at different pressures are given in Table 2.

Since no interfacial tension data of the *n*-HD–CO_2 mixture are available in the open literature, they are estimated from surface tension of pure CO_2 and pure *n*-HD through the following steps:

(1) *Find the surface tensions of pure CO_2 and pure n-HD.* At room temperature (25 °C), the surface tensions of pure CO_2 and pure *n*-HD are approximately 0.5 and 30 mN/m, respectively (Virnau et al., 2004).

(2) *Estimate the surface tension of each phase (Phase n-HD with dissolved CO_2 and Phase CO_2 with dissolved n-HD) in the n-HD–CO_2 liquid–liquid system.* The surface tension of a mixture can be estimated from surface tensions of pure components by a general formula (Poling et al., 2000)

$$\gamma_m^r = \sum_i^n X_i \gamma_i^r \tag{1}$$

where γ is the surface tension, X is the molar fraction of component i, subscript i denotes component i, subscript m indicates a mixture, superscript r is a nonlinear factor, and n is the total number of components. In this analysis, r is chosen to be 1 and molar fraction X is from experimental phase equilibrium data (Scheidgen, 1997; Polishuk et al., 2003).

(3) *The interfacial tension is approximated to be equal to the difference between surface tensions of n-HD–CO_2 mixtures estimated in the step (2).*

Estimate of the interfacial tensions of equilibrated *n*-HD–CO_2 mixtures at pressures from 10 to 25 MPa is given in Table 3. The interfacial tension decreases from 5.61 to 2.80 mN/m as pressure increases from 10 to 25 MPa. For pressures above 25 MPa, no estimate is made due to a lack of phase equilibrium data. It is worth pointing out that if two liquid phases have the same composition,

Table 2
Densities and viscosities of liquid CO_2 and *n*-HD at 25 °C.

P (MPa)	Density (kg/m^3)		Viscosity (10^{-5} Pa s)	
	CO_2[a]	*n*-HD[b]	CO_2[c]	*n*-HD[d]
10	818	773	7.5	250
15	877	773	8.7	250
20	914	773	9.5	250
25	943	773	10.3	250
30	967	773	11.0	250

[a] Data from Span and Wagner (1996).
[b] Data provided by the manufacturer.
[c] Data calculated by SUPERTRAPP (NIST, 2003).
[d] Data extrapolated from experimental data (Matthews et al., 1987).

Table 3
Estimate of interfacial tensions of equilibrated *n*-HD–CO_2 mixtures at 25 °C.

P (MPa)	γ[a] (mN/m)		Phase *n*-HD with dissolved CO_2			Phase CO_2 with dissolved *n*-HD			$\Delta\gamma_m$ (σ) (mN/m)
	CO_2	*n*-HD	X_{CO_2}[b]	$X_{n\text{-HD}}$[b]	$\gamma_{m,1}$ (mN/m)	X_{CO_2}[b]	$X_{n\text{-HD}}$[b]	$\gamma_{m,2}$ (mN/m)	
10	0.5	30	0.800	0.200	6.40	0.990	0.010	0.80	5.61
12.5	0.5	30	0.810	0.190	6.11	0.980	0.020	1.09	5.02
15	0.5	30	0.830[c]	0.170	5.52	0.965	0.035	1.53	3.98
17.5	0.5	30	0.850	0.150	4.93	0.970	0.030	1.39	3.54
20	0.5	30	0.850	0.150	4.93	0.970	0.030	1.39	3.54
22.5	0.5	30	0.875	0.125	4.19	0.970	0.030	1.39	2.80
25	0.5	30	0.875	0.125	4.19	0.970	0.030	1.39	2.80

[a] Data from Virnau et al. (2004).
[b] Data from Scheidgen (1997) and Polishuk et al. (2003).
[c] Value interpolated.

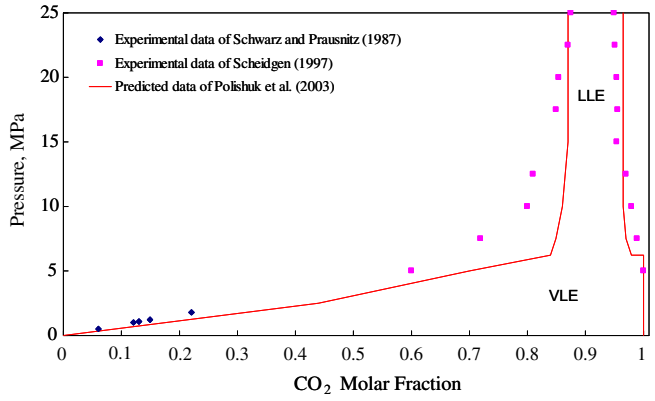

Fig. 2. *n*-HD–CO_2 phase equilibria at 25 °C. LLE: liquid–liquid equilibrium; VLE: vapor–liquid equilibrium. (See above-mentioned references for further information.)

the interfacial tension between them vanishes, no matter what this composition is. Any factor which changes phase composition changes interfacial tension of the system. This also implies that pressure affects interfacial tension by changing phase compositions.

Solubility of CO_2 in *n*-HD increases as pressure increases and temperature decreases (Sebastian et al., 1980; Charoensombut-Amon et al., 1986; Tanaka et al., 1993) and is greater than 0.5 mole fraction at 25 °C under pressures above 10 MPa (Polishuk et al., 2003), while solubility of *n*-HD in liquid CO_2 is very small (D'Souza et al., 1988) and can be neglected. A phase equilibrium diagram of the *n*-HD–CO_2 system at 25 °C given in Fig. 2 illustrates the significant impact of pressure on *n*-HD–CO_2 mutual solubility.

2.2. Flow pattern detection method

Although a variety of techniques have been developed for flow pattern determination, none of them can readily be applied in this work where severe restrictions are set by a small pipe diameter (0.0015 m I.D.) and high pressures up to 30 MPa. No probe techniques have been reported in the open literature, which can be used for determination of flow patterns in pipes of such a small diameter and under high pressure. Although the photographic technique is non-intrusive, it requires a transparent wall to access the flow field. No transparent pipes, however, can withstand pressure as high as required for this investigation. Thus, modifications of current techniques or exploration of new techniques are necessary.

After extensive search and careful comparison of different detection techniques, the photographic technique accompanied by a high-pressure view cell is considered the most suitable and reliable one for current application. Designed and constructed in this lab, the high pressure cell with two sapphire windows in opposite sides provides the capability to obtain flow pattern information inside small pipes under high pressure. Details of the equipment are described in the following section. It should be pointed out that the addition of a view cell introduces an expansion section to the pipeline, which, more or less, brings interruption to the flow field. Thus, good care must be taken when applying this method for identification of flow patterns inside small pipes or other flow phenomena studies.

In this work, the expansion effect is considered to be minimized by three aspects. First, as the pressure in the view cell is approximately the same as the inlet and outlet flow stream, expansion issues due to lowering of pressure should not change the basic flow patterns significantly. Second, although the loss of confining wall effects to the shear field of the flowing fluids changes the flow patterns downstream of the pipe somewhat, the basic flow structure is preserved and the flow pattern in the pipe can be discerned. This results because the length scale of the view cell is of the same order of magnitude as that of the pipe and the flow is in the laminar flow region with low flow velocity. Finally, we use the flow pattern observed in the view cell to predict the flow structure in the pipe before exiting the pipe into the view cell. Known flow patterns were "deduced" from the visual observations of the exiting flows even though they become distorted, somewhat, as the flow enters the view cell region. While these are judgmental evaluations, they are based on continuous flow observations instead of evaluation of one single image in the view cell and the flow patterns can be predicted satisfactorily.

2.3. Experimental setup

The experimental setup comprises of three sections: the fluid delivery section, the flow visualization section, and the pressure control section. A schematic diagram of the experimental setup is shown in Fig. 3. Descriptions of main equipment are given in Table 4. In the fluid delivery section, *n*-HD and liquid CO_2 were pressurized and then delivered by a solvent delivery system and a syringe pump, respectively. Two liquids impinged in the mixing tee, mixed downstream in the mixing pipe, and then entered into a high-pressure view cell where flow patterns were observed and recorded by the flow visualization system.

The flow visualization section includes the high-pressure view cell, a CCD camera with a macro-lens, and a data acquisition unit installed in a computer. The high-pressure view cell is a key component of the visualization section. It was constructed in a high pressure cross with two sapphire windows in opposite sides and can withstand pressures up to 60 MPa and temperatures up to 450 °C at the same time. The structure and dimensions of the view cell is given in Fig. 4. More details are available elsewhere (Lin,

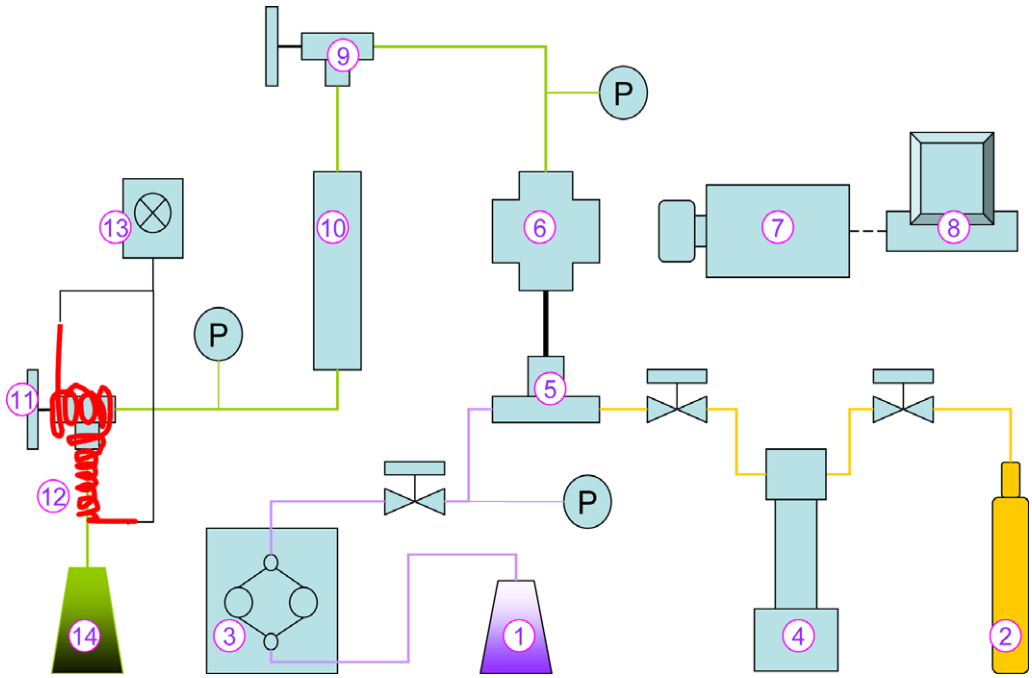

Fig. 3. A schematic diagram of the experimental setup. (1) *n*-HD reservoir, (2) CO_2 cylinder, (3) solvent delivery system, (4) syringe pump, (5) mixing tee, (6) view cell, (7) CCD camera, (8) computer, (9) and (11) micro-metering valves, (10) high pressure vessel, (12) heating tape, (13) temperature controller, (14) recycle reservoir, (*P*) pressure gauge/transducer.

Table 4
Main equipment used in the flow pattern determination experiment.

Name	Description	Manufacturer
Solvent delivery system	Dynamax Model SD-1	Rainin
Syringe pump	Model 100D	Teledyne ISCO
View cell	High pressure cross, stainless steel	HiP
Sapphire window	0.0127 m diameter, 0.00635 m Thickness	Meller Optics
Monochrome frame transfer CCD camera	Solid state camera, Model 4812–5000	COHU
Macro-lens	55 mm, *f*2.8	Vivitar
Micro-metering valve	0.00318 m Tube OD, 0.00157 m D Orifice	Autoclave
High pressure vessel	0.0001 m^3, 69 MPa at 90 °C	TharTech
Mixing tee	SS Union tee, 0.00318 m Tube OD	Swagelok
Heating tape	XtremeFLEX® BWH heavy insulated heating tapes, W0.0254 m, L1.9 m, 470 W	BriskHeat Products
Temperature controller	TP0 Portable time percentage dial temperature controller, 120 V, 15 A, 5–100%	BriskHeat Products
Pressure transducer	Model HPO	HEISE
Pressure indicator	Model 901A	HEISE
Pressure gauge	Model CM, 0/52 MPa	HEISE

2008). The diameter of the view field is 0.0065 m. A 4810 series monochrome frame transfer CCD camera with a maximum displaying rate of 30 frames per second was used to capture flow patterns.

Steady flow of a compressible fluid mixture under high pressure is difficult to achieve and requires precise and simultaneous control of flow rates and pressure. In this work, the inlet volumetric flow rates of liquid CO_2 and *n*-HD were measured and precisely controlled by the syringe pump with an accuracy of ±0.3% and the solvent delivery system with an accuracy of ±0.5%, respectively. *n*-HD–CO_2 continuous flow was considered to reach steady state when a constant pressure was maintained in the system. To achieve a constant pressure, a 0.0001 m^3 high pressure vessel was placed into the system between two micro-metering valves, which increased the total volume of the system and hence minimized pressure fluctuation resulting from changes of outlet flow rate. Moreover, when the *n*-HD–CO_2 mixture is released under high pressure, fluid temperature drops rapidly down to the freezing point of CO_2 due to the cooling effect of CO_2 evaporation and CO_2 is easily solidified and blocks the pipe. Thus, as shown in Fig. 3, a heating tape was coiled around the micro-metering valve to prevent CO_2 solidification. By applying these strategies, *n*-HD–CO_2 liquid–liquid two-phase steady flow under high pressure was achieved.

2.4. Experimental conditions and procedure

Observations of flow patterns of *n*-HD–CO_2 liquid–liquid two-phase flow were made in two 0.0015 m I.D stainless steel pipes of lengths 0.068 m and 0.5 m with corresponding *L*/*D* ratios of 45 and 333; 0.068 m was the minimum length available to access flow patterns as close to the entrance as possible. The total volumetric flow rate was fixed at 2.0×10^{-6} m^3/min, while the flow rate ratio (φ) which is given by

$$\varphi = \frac{Q_{CO_2}}{Q_{n\text{-HD}}} \tag{2}$$

varied from 0.05 to 19. The experimental conditions are summarized in Table 5 and different combinations of flow rates of *n*-HD and CO_2 are given in Table 6.

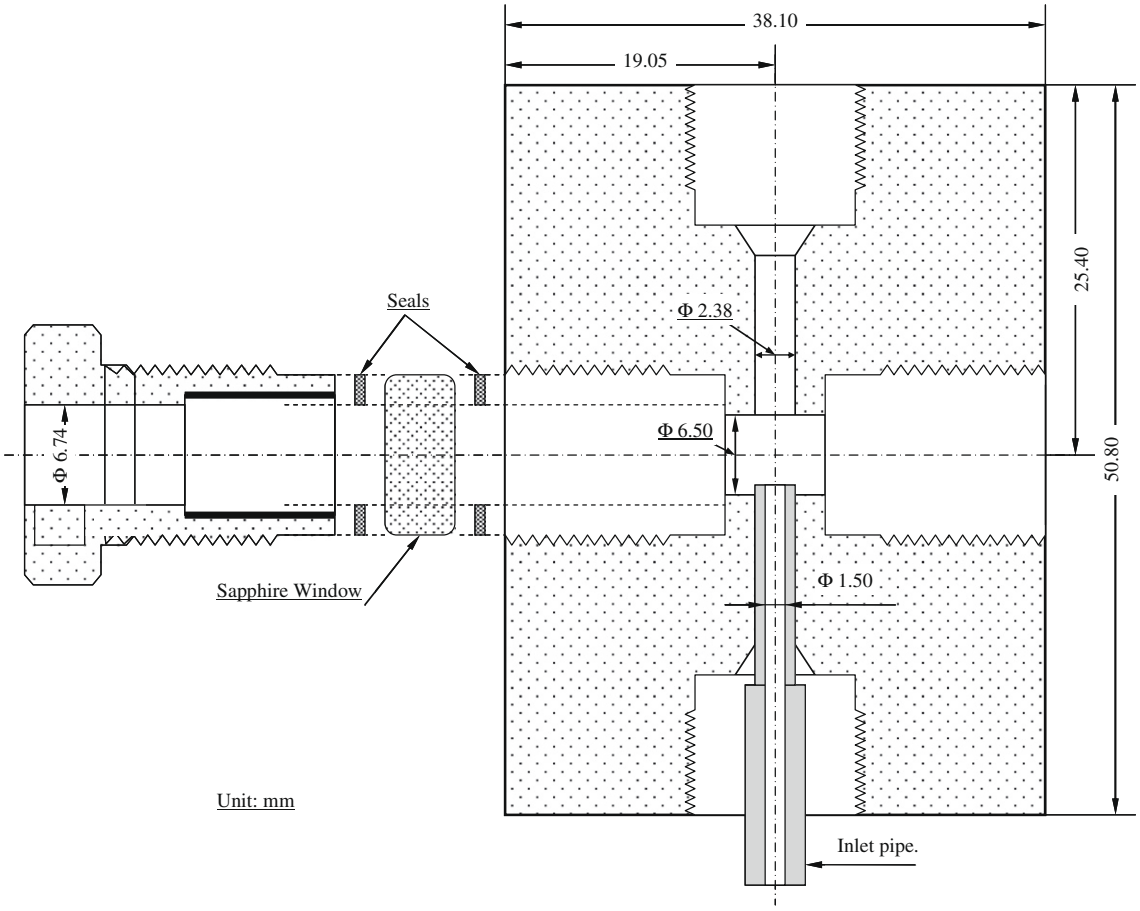

Fig. 4. Structure and dimensions of the high-pressure view cell.

Table 5
Experimental conditions.

Temperature (°C)	23–25
Pressure (MPa)	10.3–29.6
Diameter of mixing pipes (m)	0.0015
Length of mixing pipes (m)	0.068, 0.5
L/D ratios	45, 333
Volume of the view cell (m^3)	2.02×10^{-7}
Total flow rate (m^3/min)	2.0×10^{-6}
Estimated mixture velocity (m/min)	1.13
Estimated Reynolds number	10–320

Experiments were carried out as follows. Liquid CO_2 was pumped initially to build high pressure in the system to a maximum value (29.6 MPa) and then *n*-HD was introduced. Flow rates of liquid CO_2 and *n*-HD were set for a given flow rate ratio according to Table 6. Steady flow was achieved at a given pressure within a fluctuation of 0.03 MPa by controlling the opening of two micro-metering valves. At a given flow rate ratio, observations of flow patterns were made by decreasing pressure with an interval of 1.38 MPa at higher pressure and 0.69 MPa at lower pressure. The pressure difference between the view cell and the high pressure vessel was maintained within 1.38 MPa. After taking images at a certain pressure and a given flow rate ratio, pressure was reduced to the next lower value by opening the two micro-metering valves. When repeated flow pattern images appeared in the view cell, the flow reached the steady state and flow pattern images were recorded. Following the above procedure, flow patterns of *n*-HD–CO_2 liquid–liquid two-phase upward flow in vertical pipes were observed and recorded at a given flow rate ratio varying from 0.05 to 19 under high pressures decreasing from 29.6 to 10.3 MPa.

3. Results and discussions

3.1. Flow patterns

Flow patterns were determined by analyzing a sequence of images captured by the CCD camera under different flow conditions. Since the length scale of the view cell (0.0065 m) was larger than the pipe I.D. (0.0015 m), the flow was interrupted by the addition of view cell to the pipe somewhat. Thus, flow patterns in the pipe were determined by carefully examining the flow behavior leaving the mixing pipe. Fluid movement under each set of conditions was recorded in a sequence of images, and then by analyzing flow movement, information of flow patterns in the pipe was ex-

Table 6
Flow rate conditions for the flow pattern determination experiment.

Flow rate, Q ($\times 10^{-6}$ m^3/min)	CO_2	0.1	0.2	0.3	0.4	0.5	0.6	0.8	1.0	1.2	1.4	1.5	1.6	1.7	1.8	1.9
	n-HD	1.9	1.8	1.7	1.6	1.5	1.4	1.2	1.0	0.8	0.6	0.5	0.4	0.3	0.2	0.1
Flow rate ratio, φ		0.05	0.11	0.18	0.25	0.33	0.43	0.67	1.00	1.50	2.33	3.00	4.00	5.67	9.00	19.0

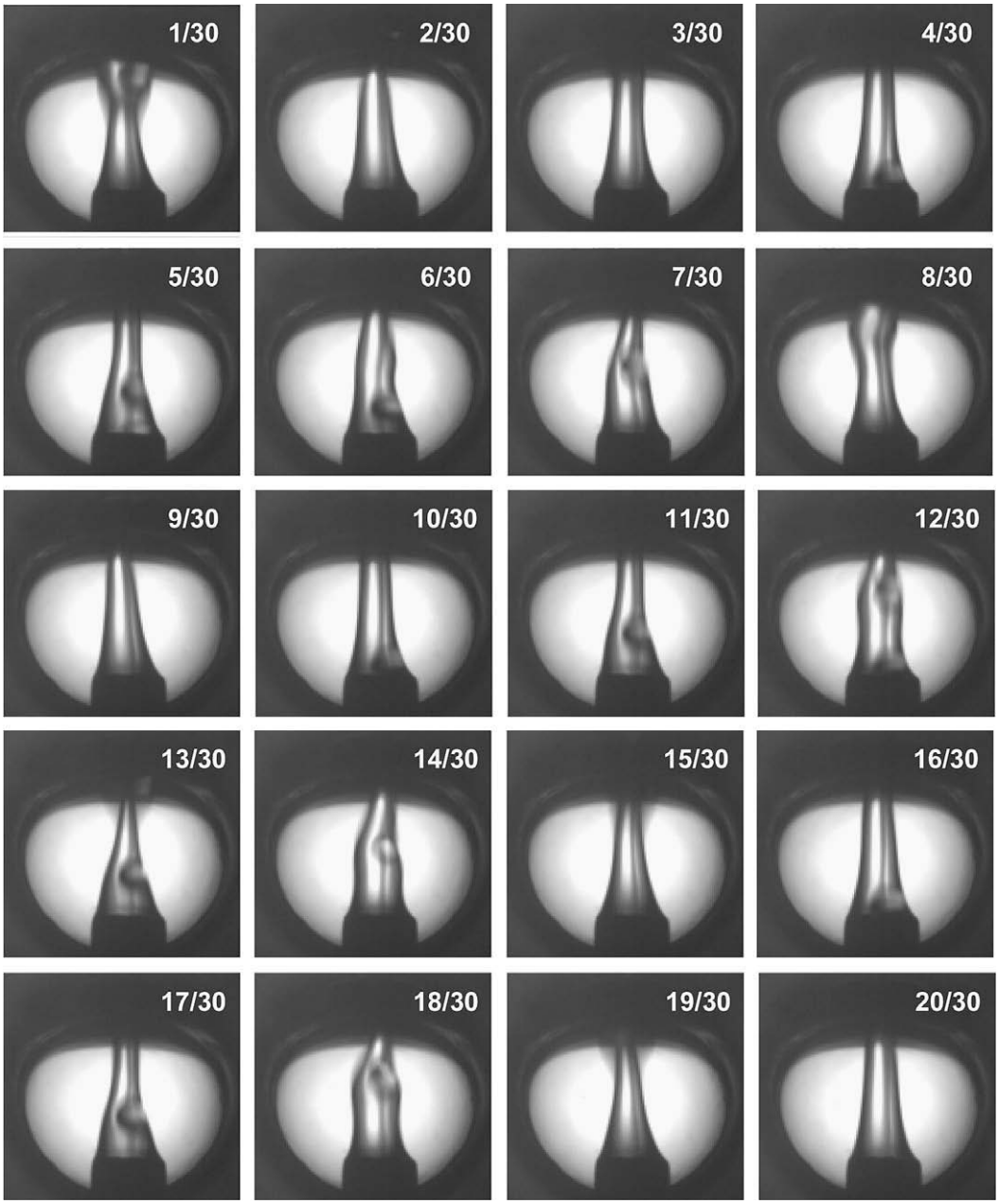

Fig. 5. Temporal sequence of bubbly flow pattern images at $Q_{CO_2} = 0.2 \times 10^{-6}$ m^3/min and $Q_{n\text{-HD}} = 1.8 \times 10^{-6}$ m^3/min at $P = 11.4$ MPa.

tracted. A sequence of bubbly flow pattern images is given in Fig. 5 for illustration. These images were recorded in the movie mode of a frame displaying rate of 30 frames per second. Shown in these images are liquid CO_2 which appears white filling the view cell and the *n*-HD main stream shown in dark flowing out of the mixing pipe (bottom) and into the outlet of the view cell (top) with some liquid CO_2 droplets inside the stream. Due to different refractive index resulting from a density difference between CO_2 and *n*-HD, liquid CO_2 droplets were clearly observed in the main stream. Similar images were recorded for all conditions.

Seven different flow patterns were observed in the 0.068 m pipe. They are bubbly flow, plug flow, slug flow, annular flow, stratified flow, transitional region, and near-one-phase region. In the 0.5 m pipe, five flow patterns were identified, leaving one region undetermined due to the limitation of the facility. The five flow patterns observed in the 0.5 m pipe include bubbly flow, plug flow, slug flow, annular flow, and near-one-phase flow region. Selected images of each flow pattern except the transitional and the undetermined regions are demonstrated in Fig. 6 for the 0.068 m pipe and Fig. 7 for the 0.5 m pipe. Also shown in Figs. 6 and 7 are sketches of flow pattern configurations in the pipe. They are added for a better demonstration.

3.1.1. Bubbly flow

Bubbly flow was found in both pipes as shown in Fig. 6A for the 0.068 m pipe and in Fig. 7A for the 0.5 m pipe. Bubbly flow identified in this work is characterized by small CO_2 droplets scattering in the *n*-HD stream with droplet size less than pipe I.D. but of the same order of magnitude. Shown in the view cell in both Figs. 6A and 7A are two layers, CO_2 on the bottom and *n*-HD on the top, and a *n*-HD stream containing CO_2 droplets coming out of the mixing pipe, passing through the interface, and entering into the outlet of the view cell. It was found that as flow rate ratio increased, the size of CO_2 droplets increased slightly.

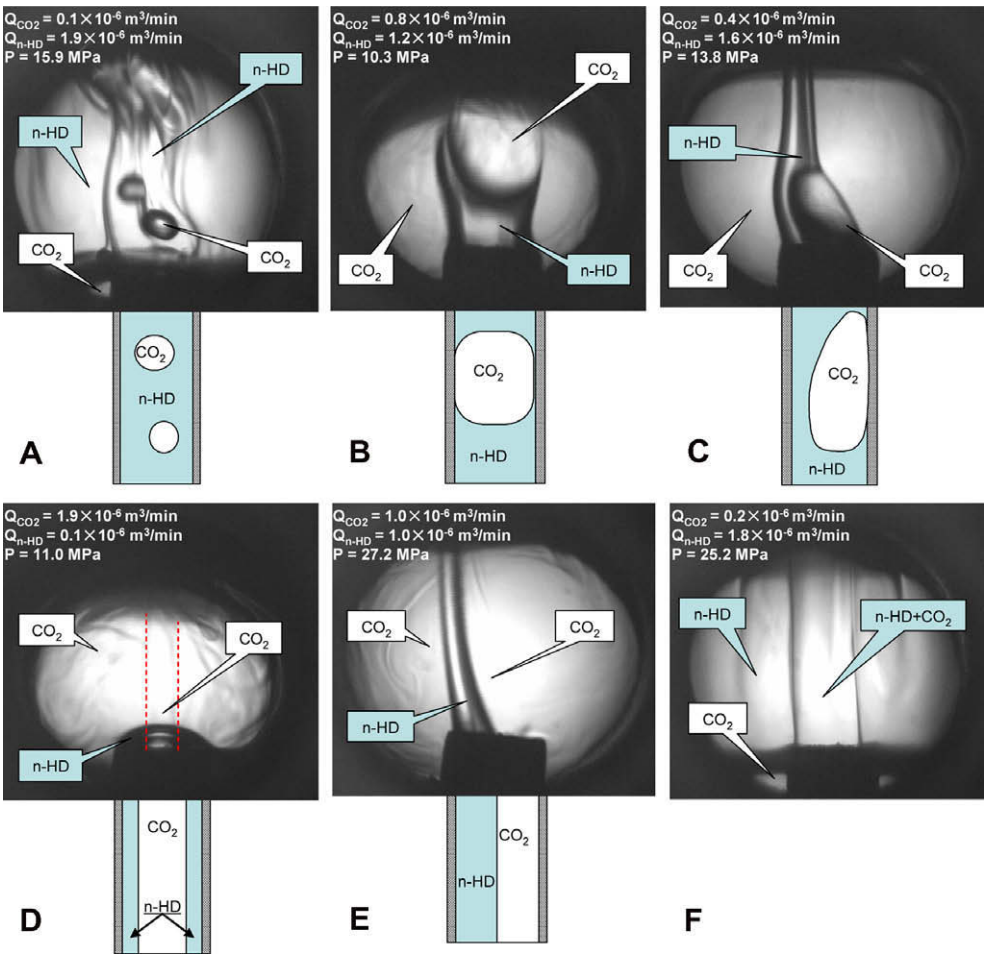

Fig. 6. Flow patterns observed in the 0.068 m pipe. (A) Bubbly flow, (B) plug flow, (C) slug flow, (D) annular flow, (E) stratified flow, (F) near-one-phase flow.

3.1.2. Plug flow

At a given pressure, as flow rate ratio increased, bubbly flow was observed to transition to plug flow in both pipes. This may be explained that as flow rate ratio increases, the size of CO_2 droplets increases, which may be due to coalesce of adjacent droplets. When the diameter of CO_2 droplet exceeds inner diameter of the pipe, plug flow forms. Shown in Figs. 6B and 7B are appearances of plug flow in the view cell for the 0.0068 m pipe and the 0.5 m pipe, respectively. As flow rate ratio and pressure changed, different forms of CO_2 plugs were observed in the view cell.

3.1.3. Slug flow

Slug flow was also found in both pipes as shown in Fig. 6C and 7C. Different to plug flow, slug flow is characterized by large elongated CO_2 slugs eccentrically attaching to the pipe. For flows initially in the bubbly or plug flow region at a given flow rate ratio, it was found that the flow transitioned to the slug flow as pressure increased. Fig. 8 shows a transition from bubbly flow to slug flow.

3.1.4. Annular flow

Annular flow occurred at high flow rate ratios in both pipes. As CO_2 flow rate increased, the distance between two plugs or slugs decreased. When CO_2 flow rate increased to 1.0×10^{-6} m^3/min and above, the amount of liquid CO_2 was enough to form a core flow surrounded by the *n*-HD annular flow. Since the view cell was filled with CO_2, the CO_2 core flow was not clearly captured in flow pattern images. In Fig. 6D, the CO_2 core flow indicated by two red dash lines was located in the middle, while the *n*-HD annular flow appears as a dark overflow along the pipe. Evidence of annular flow can also be found in Fig. 7D for the 0.5 m pipe where *n*-HD distributed along the pipe.

3.1.5. Stratified flow

Stratified flow was only observed in the 0.068 m pipe. For initial annular flow, when pressure increased, the annular *n*-HD accumulated on one side of the pipe, forming stratified flow. Shown in Fig. 6E is the stratified flow where the *n*-HD layer appears in dark on the left and the CO_2 layer appears in white on the right, merging with the CO_2 in the view cell. When the pipe length was increased to 0.5 m, no stratified flow was identified. It is reasonable to conclude that stratified flow is an entrance phenomenon in vertical upward pipe flow.

3.1.6. Near-one-phase flow region

Near-one-phase flow appeared in both pipes at low flow rate ratio and high pressure. A similar flow pattern also occurred at very high flow rate ratio in the 0.5 m pipe. This flow behavior is considered to be due to the mutual solubility of *n*-HD and liquid CO_2. It is also shown that flows in the 0.5 m pipe (Fig. 7E) were more homogenized than that in the 0.068 m pipe (Fig. 6F), which verifies the effect of solubilization. As the pipe length increases, mixing time increases, and hence, more CO_2 or *n*-HD dissolves into *n*-HD or CO_2.

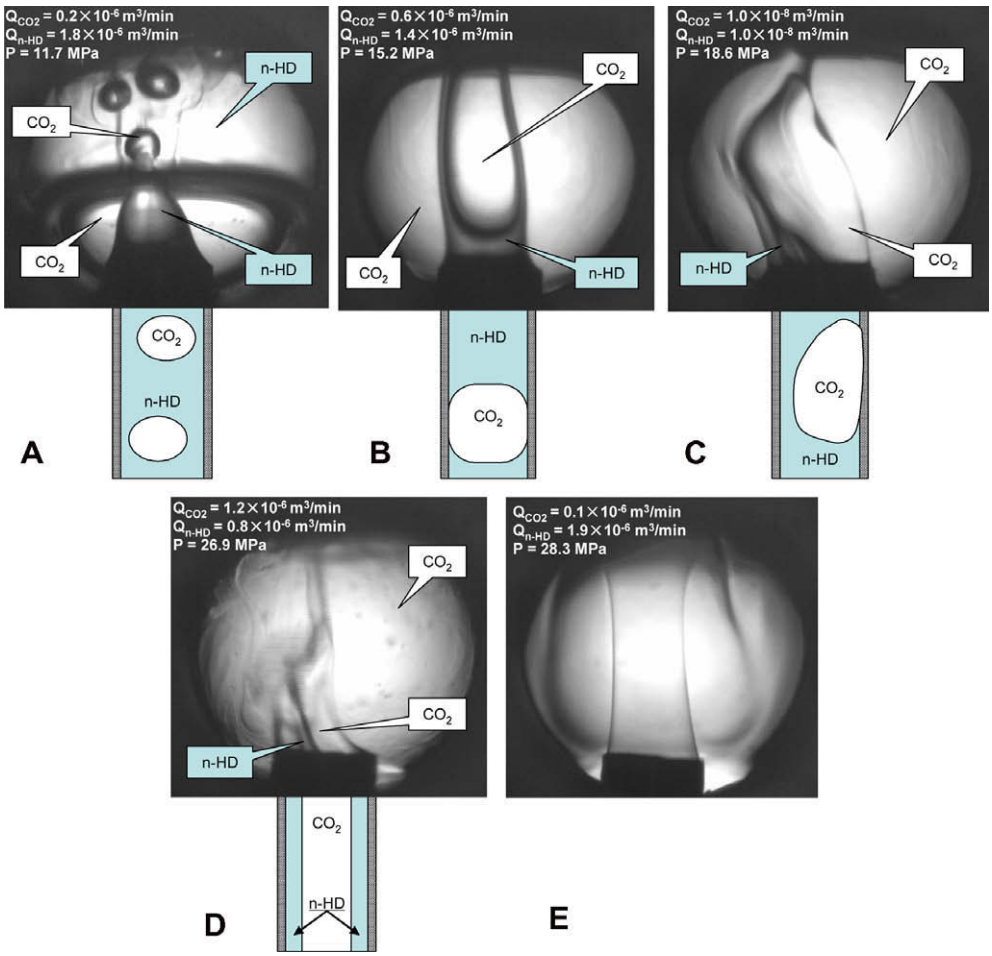

Fig. 7. Flow patterns observed in the 0.5 m pipe. (A) Bubbly flow, (B) plug flow, (C) slug flow, (D) annular flow, (E) near-one-phase flow.

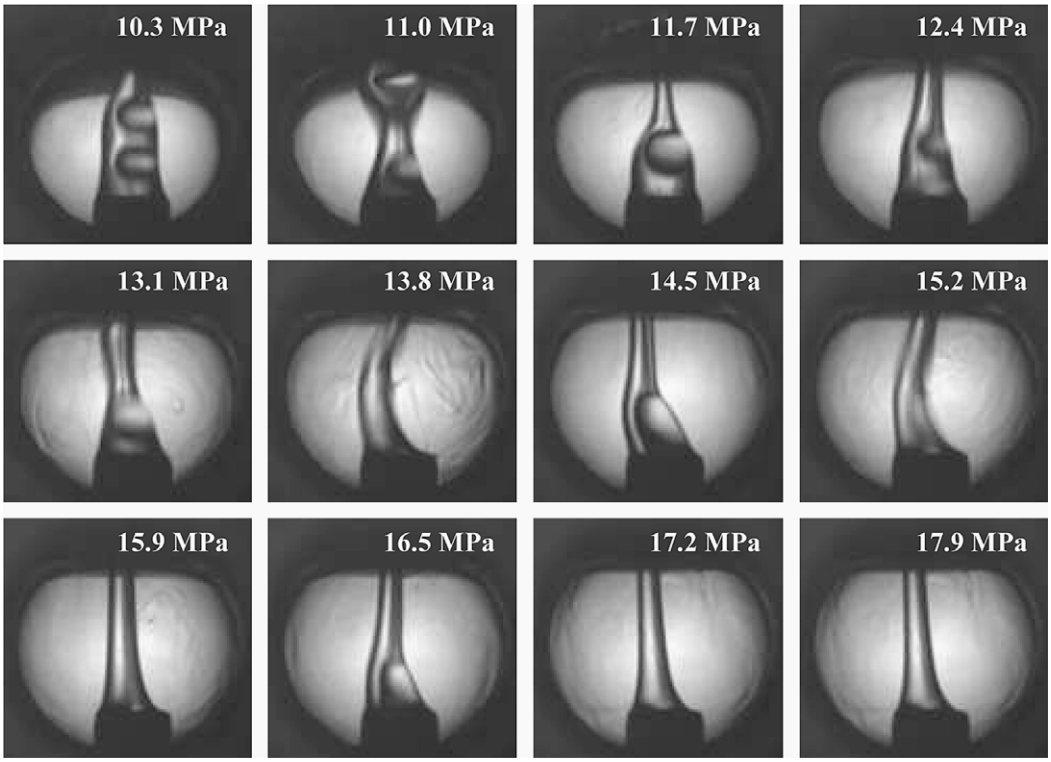

Fig. 8. Change in flow patterns in the 0.068 m pipe under different pressures at $Q_{CO_2} = 0.4 \times 10^{-6}$ m^3/min and $Q_{n\text{-HD}} = 1.6 \times 10^{-6}$ m^3/min ($\phi = 0.25$).

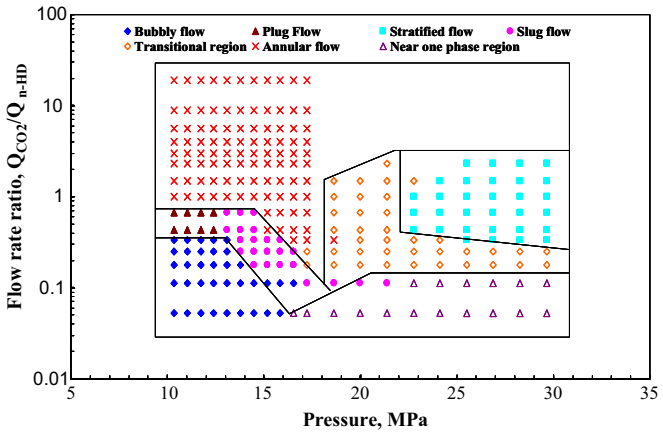

Fig. 9. A flow pattern map of *n*-HD–CO_2 liquid–liquid two-phase vertical upward flow in a stainless steel pipe of I.D 0.0015 m and length 0.068 m.

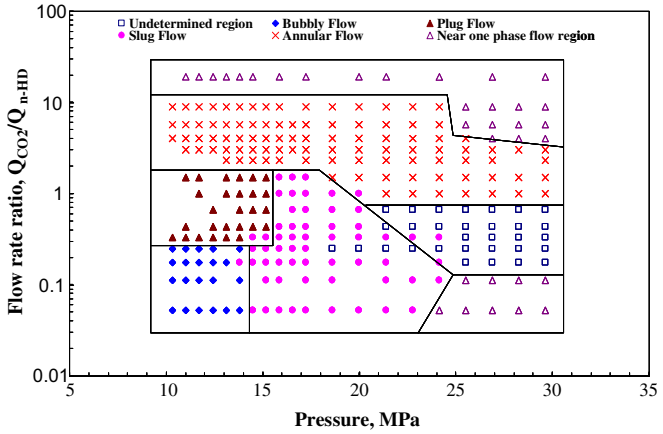

Fig. 10. A flow pattern map of *n*-HD–CO_2 liquid–liquid two-phase vertical upward flow in a stainless steel pipe of I.D 0.0015 m and length 0.5 m.

3.2. Flow pattern maps

Flow pattern maps for both pipes were constructed by plotting flow patterns in the flow rate ratio versus pressure diagrams. Such maps for the 0.068 m and the 0.5 m pipes are shown in Figs. 9 and 10, respectively. Different to other flow pattern maps reported in the literature (Jana et al., 2006a; Wegmann and von Rohr, 2006), these maps demonstrate significant impacts of both flow rate ratio and pressure on flow patterns.

For the 0.068 m pipe, as shown in Fig. 9, bubbly flow was observed in a range of flow rate ratios from 0.05 to 0.33 and at pressures below 16.5 MPa. As flow rate ratio increased, bubbly flow transfers to plug flow at pressure below 12.4 MPa and to slug flow when pressure was above 12.4 MPa, and then entered into the annular flow regime. When pressure increased to above 16.5 MPa, near-one-phase flow formed in the low flow rate ratio end due to the dissolution of CO_2 into *n*-HD. Flow patterns transferred from the near-one-phase flow region, to slug flow, and then annular flow or transitional region at pressures between 15.9 and 21.4 MPa as flow rate ratio increased. Whereas at pressure increased above 22.8 MPa, flow patterns changed from the near-one-phase flow to the transitional region and then from the transitional region to stratified flow as flow rate ratio increased.

In the 0.5 m pipe, as shown in Fig. 10, bubbly flow occurred at flow rate ratio below 0.33 ($Q_{CO_2} = 0.5 \times 10^{-6}$ m^3/min and $Q_{n\text{-HD}} = 1.5 \times 10^{-6}$ m^3/min) and pressure less than 14.5 MPa. When increasing the flow rate ratio above 0.33–1.50, plug flow dominated. Further increasing the flow rate ratio, plug flow transitioned to annular flow with liquid CO_2 in the core and *n*-HD in the annulus. Finally, the flow became almost one-phase flow since the *n*-HD flow rate was so small that it almost completely dissolved into CO_2. When increasing the pressure, both bubbly flow and plug flow became slug flow, while annular flow kept the same flow pattern. At pressures above 24.1 MPa, flow patterns changed from near-one-phase flow to annular flow via an undetermined region and then to near-one-phase flow again as flow rate ratio increased.

3.3. Effect of flow rate ratio on flow patterns

Flow pattern maps in Figs. 9 and 10 clearly demonstrate the effect of flow rate ratio on flow patterns. At low pressures where the impact of pressure on flow patterns is not that significant, flow patterns transition from bubbly to plug and then to annular flow as flow rate ratio increases. This trend of transition agrees well with previous studies (Jana et al., 2006a). It can be seen that bubbly or annular flow is inclined to occur as the flow rate ratio moves away from unity. However, whether bubbly or annular will occur depends on fluid properties. If the fluid of lower flow rate tends to wet the pipe wall, annular flow forms, otherwise bubbly flow forms. Fig. 11 shows change in flow patterns in the 0.5 m pipe at 13.8 MPa as flow rate ratio increased from 0.05 to 19.0. Note that in the annular regions (φ = 2.33–9.0) *n*-HD merged to form a drop as it rose from the exit to the mixing pipe.

The mechanism of formation of different flow patterns, particularly bubbly, plug, slug, and annular flows, can be explained by the instability of stratified flow as illustrated in Fig. 12. It is generally understood that stratified flow is unstable in vertical pipes. At low flow rate ratio, the thin layer of phase B as indicated in Fig. 12 breaks and shrinks to form drops. As flow rate ratio increases to near unity, the layer of phase B still breaks, but forming large plugs or slugs. As flow rate ratio increases further, phase A creeps around the wall, while phase B becomes core flow.

3.4. Effect of pipe length on flow patterns

A comparison of flow patterns in both pipes was made in Fig. 13 where the red solid line indicates flow pattern transitions in the 0.068 m pipe, while the blue dash line denotes flow pattern transitions in the 0.5 m pipe. Bubbly, slug, plug, and annular flows were found in the similar region in the flow pattern maps for both pipes. Compared to the flow patterns in the 0.068 m pipe, the bubbly flow region in the 0.5 m pipe was shrunk, while the plug and slug flow regions were extended, which may suggest that the formation of plug or slug flow is partially due to the coalescence of CO_2 droplets.

The near-one-phase flow region was found in both the lower and the higher flow rate ratio regions in the 0.5 m pipe, while it was only observed in the lower flow rate ratio region in the 0.068 m pipe. This phenomenon may imply the impact of mixing time on flow patterns. As residence time increases, mutual solubilization of *n*-HD and CO_2 is enhanced, which further affects the flow rate ratio of two phases in the pipe. This was confirmed by the appearance of near-one-phase flow in the higher flow rate ratio region. In the lower flow rate ratio region, however, the range of the near-one-phase flow region was reduced. Further investigation is required to address this phenomenon.

Stratified flow was recognized only in the 0.068 m pipe, and under the same operation conditions, it appeared to be annular flow in the 0.5 m pipe. This behavior most likely occurred because flow in the 0.068 m pipe was still under development and not stabilized.

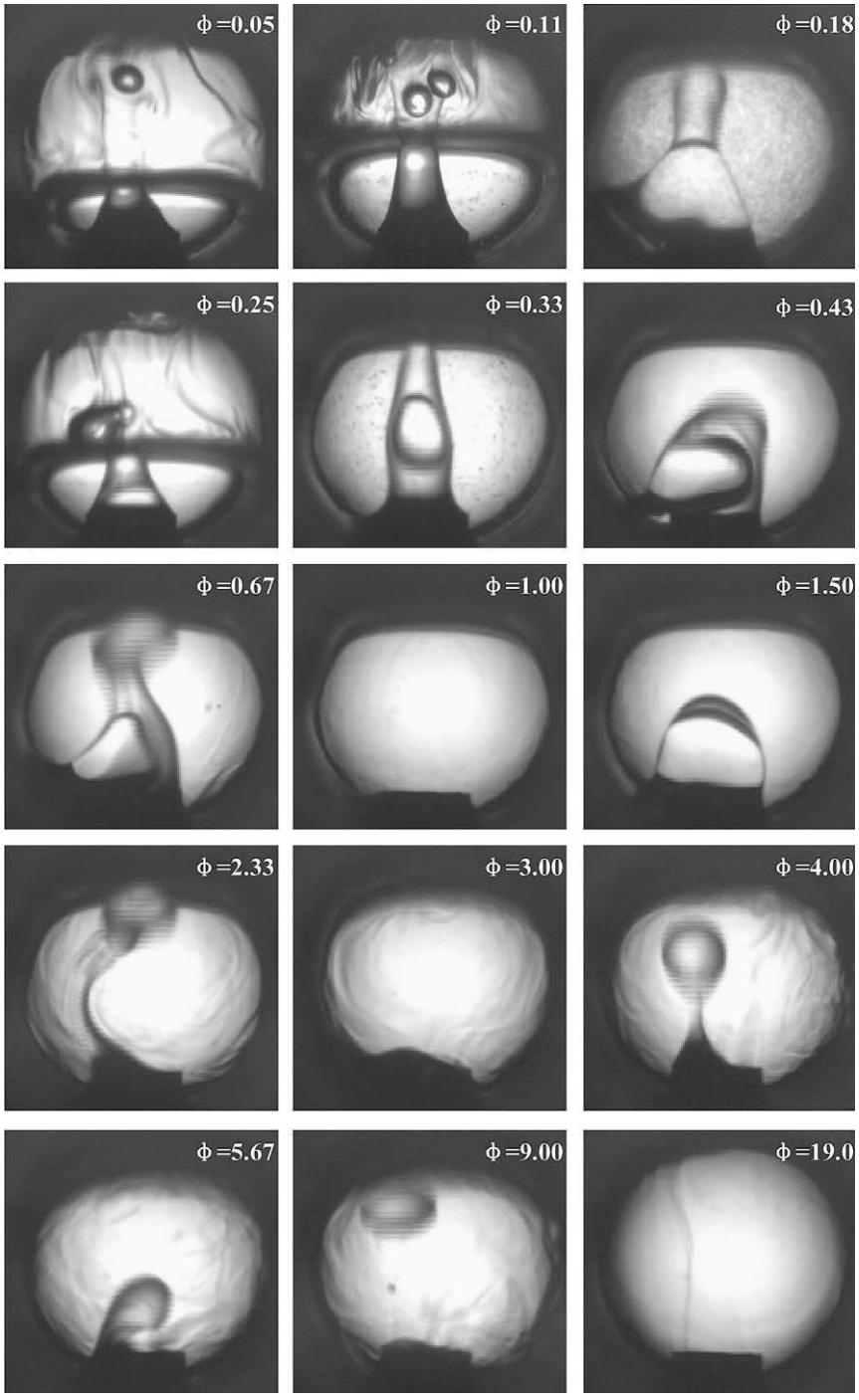

Fig. 11. Change in flow patterns in the 0.5 m pipe at different flow rate ratios at P = 13.8 MPa.

However, predicted by an analytical relationship (Durst et al., 2005), the maximum L/D ratio for laminar flow entrance length under current experimental conditions is approximately 18, which is less than experimental L/D ratios. This difference suggests that further investigations are essential to understand flow development and entrance phenomena, especially for multiphase flows.

3.5. Effect of pressure on flow patterns

The impact of pressure on flow patterns is not well understood and was seldom discussed in the literature. Ujang et al. (2006) studied slug initiation and evolution in gas–liquid two-phase horizontal flow under different pressures and found that increasing gas pressure had the effect of suppressing wave growth, resulting in a delay of slug initiation. Omebere-Iyari et al. (2007) investigated flow patterns of naphtha-nitrogen system under high pressures and found that flow pattern transition lines shifted as pressure increased from 2 to 9 MPa. For liquid–liquid two-phase flow, almost all previous investigations were focused on low pressures.

In this study, it was observed that at a given flow rate ratio, flow pattern transitions occurred in both pipes as pressure increased. As shown in Fig. 13, bubbly flow and plug flow became unstable and transitioned to slug flow in both cases as pressure increased, while

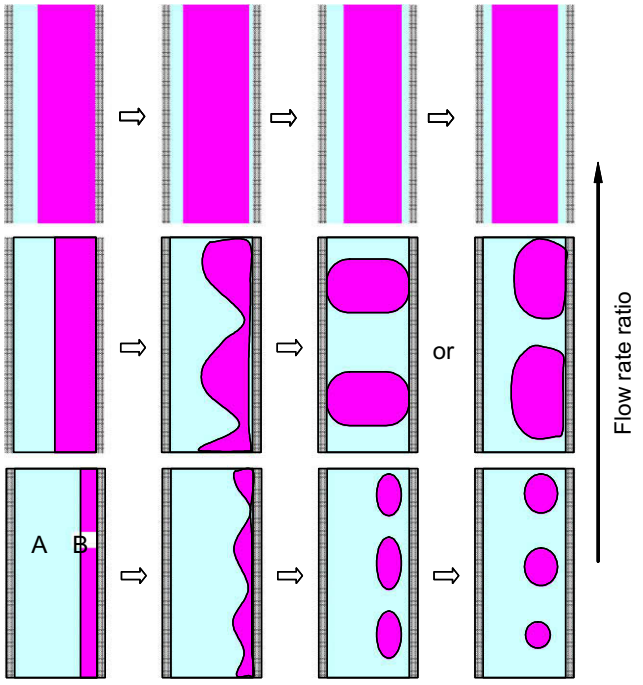

Fig. 12. Formation of different flow patterns.

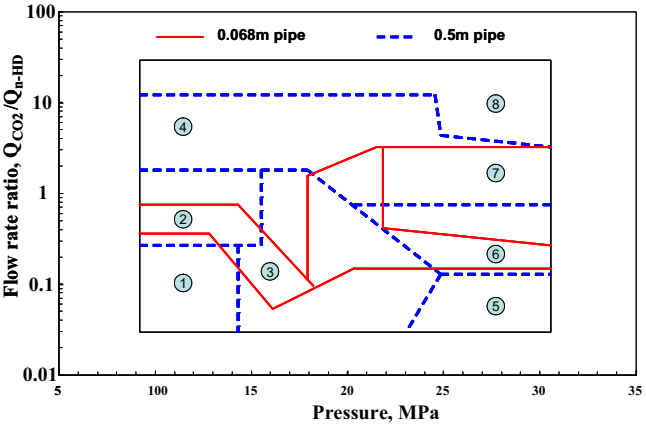

Fig. 13. Comparison of flow patterns in the 0.068 m and 0.5 m pipes. (1) Bubbly flow region, (2) plug flow region, (3) slug flow region, (4) annular flow region, (5) and (8) near-one-phase flow region, (6) transitional (0.068 m pipe) or undetermined (0.5 m pipe) region, and (7) stratified (0.068 m pipe) or annular (0.5 m pipe) flow region.

annular flow was more stable than bubbly and plug flows over a wider range of pressure. Near-one-phase flows were observed under high pressures when flow rate ratio was far away from unity.

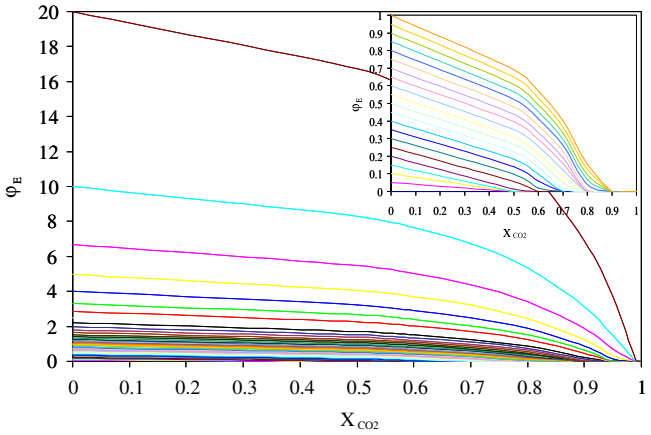

Fig. 14. Effect of the solubility of CO_2 in *n*-HD on flow rate ratio (φ_E) of two phases in equilibrium. Inset: flow rate ratio in the range of 0–1.

These phenomena suggest that pressure may influence flow patterns through its impact on fluid properties such as solubility, density, and interfacial tension.

Solubility may affect flow pattern by changing flow rate ratio of two liquid phases in the pipe. For two immiscible liquids, flow rate ratio of two phases in the pipe equals the initial flow rate ratio of the two liquids. For partially miscible liquids, however, flow rate ratio of two phases in the pipe changes as solubilization occurs along the flow. Fig. 14 shows decreases of flow rate ratio of two phases in equilibrium in the pipe as the solubility of CO_2 in *n*-HD increases. Data given in this figure are calculated based on mass balance of each component under thermodynamic equilibrium conditions. When the solubility of CO_2 in *n*-HD equals to zero, which means that two liquids are immiscible, flow rate ratio of two phases keeps the same as the initial flow rate ratio of two liquids. As the solubility of CO_2 in *n*-HD increases above 0.5, dramatic decreases in flow rate ratio of two phases in the pipe occur, which consequently influences flow patterns.

Moreover, the degree of solubilization is determined by residence time which is further determined by the length of mixing pipes. This was evidenced by the near-one-phase flow region observed in the 0.5 m pipe at high flow rate ratio. As CO_2 dissolved into *n*-HD, the density difference between CO_2 and *n*-HD–CO_2 mixture reduced, leading to a more uniform view field.

The influence of density and interfacial tension on flow patterns can be categorized through the non-dimensional Eotvös number (Brauner, 2004) defined by

$$Eo_D = \frac{\Delta\rho g D^2}{8\sigma} \tag{3}$$

where $\Delta\rho$ is the density difference of two liquid phases, g is the gravity acceleration constant, D is the inner diameter of the pipe,

Table 7
Estimate of Eotvös number as a function of pressure.

Pressure (P), MPa	Density (ρ), kg/m^3		g (m/s^2)	Inner diameter of the pipe (D), m	Interfacial tension[c] (σ), N/m	Eotvös number Eo_D[d]
	CO_2[a]	*n*-HD[b]				
10	818	773	9.8	0.0015	0.0056	0.02
15	877	773	9.8	0.0015	0.0040	0.07
20	914	773	9.8	0.0015	0.0035	0.11
25	943	773	9.8	0.0015	0.0028	0.17

[a] Data from Span and Wagner (1996).
[b] Data provided by the manufacturer.
[c] Value from Table 3.
[d] Value calculated using Eq. (3).

and σ is the interfacial tension. The Eotvös number characterizes the impacts of the gravitational force and the interfacial tension on flow patterns. If the Eotvös number is less than one, the system is dominated by interfacial tension, while the gravitational force plays a key role when the Eotvös number is greater than one. Estimation of the Eotvös number in a pressure range from 10 to 25 MPa is made by simply inputting density and interfacial tension data discussed in Section 2.1 into Eq. (3). Results and data used are given in Table 7. It is shown that the Eotvös number increases as pressure increases. The Eotvös number estimated is significantly below unity, which implies that interfacial tension plays a key role in determining flow patterns. However, no obvious relationship between flow patterns and the Eotvös number can be extracted from this analysis. Also, due to the limitation of experimental data, no estimate was made for pressure above 25 MPa. Further investigations are required to address these issues.

4. Conclusions

Flow patterns of *n*-hexadecane–CO_2 liquid–liquid two-phase vertical upward flow in small diameter stainless steel pipes under high pressures were observed and determined. Different flow patterns or regions observed include bubbly flow, plug flow, slug flow, annular flow, stratified flow, transitional region, and near-one-phase flow region in the 0.068 m pipe and bubbly flow, plug flow, slug flow, annular flow, and near-one-phase flow region in the 0.5 m pipe. One region in the 0.5 m pipe was undetermined due to the limitation of the facility. Flow pattern maps were constructed in the flow rate ratio versus pressure graph which reveals significant impacts of flow rate ratio, pipe length, and pressure on flow patterns. This work is the first attempt to observe complex liquid–liquid two-phase flow behavior with flow pattern transitions at high pressure.

Flow rate ratio affects flow patterns by directly changing liquid holdup and distribution. At low pressure, flow pattern transitioned from bubbly flow to plug flow and then annular flow as flow rate ratio increased. Such transition was significantly influenced by pressure. The effect of pipe length on flow patterns was also examined. Flow patterns and their transitions were found generally similar in both cases. However, stratified flow was only observed in the shorter pipe. Such phenomena are considered to be due to the impact of pipe length on residence time of two phases which further affects the extent of mutual solubilization.

The effect of pressure on *n*-hexadecane–CO_2 liquid–liquid two-phase flow patterns is believed to be due to its impact on both the mutual solubilization and the subsequent changes in interfacial tension and density which can be categorized through the non-dimensional Eotvös number. Mutual solubilization affects flow patterns by changing flow rate ratio of two phases in the pipe, which has similar effects on flow patterns as initial flow rate ratio. The Eotvös number, which determines the role of gravitational force and interfacial tension in characterizing flow patterns in pipe flow, was estimated to be 0.02–0.17 as pressure increases from 10 to 25 MPa, showing that flow pattern under current experimental conditions is determined by interfacial tension.

Acknowledgements

This work was supported by the New York State Energy Research and Development Authority (NYSERDA) under the Agreement No. 8915-1-2. The authors are grateful to Dr. Gheorghe Anitescu for the assistance in the construction of the high pressure visualization system.

Appendix A. Supplementary data

Supplementary data associated with this article can be found, in the online version, at doi:10.1016/j.ijmultiphaseflow.2009.02.008.

References

Abduvayt, P., Manabe, R., Watanabe, T., Arihara, N., 2006. Analysis of oil/water-flow tests in horizontal, hilly terrain, and vertical pipes. SPE Prod. Operations 21, 123–133.
Angeli, P., Hewitt, G.F., 1998. Pressure gradient in horizontal liquid–liquid flows. Int. J. Multiphase Flow 24, 1183–1203.
Angeli, P., Hewitt, G.F., 2000. Flow structure in horizontal oil–water flow. Int. J. Multiphase Flow 26, 1117–1140.
Beretta, A., Ferrari, P., Galbiati, L., Andreini, P.A., 1997a. Horizontal oil–water flow in small diameter tubes: flow patterns. Int. Commun. Heat Mass Transfer 24, 223–229.
Beretta, A., Ferrari, P., Galbiati, L., Andreini, P.A., 1997b. Horizontal oil–water flow in small diameter tubes: pressure drop. Int. Commun. Heat Mass Transfer 24, 231–239.
Brauner, N., 2004. Liquid–liquid two-phase flow systems. In: Bertola, V. (Ed.), Modeling and Control of Two-Phase Flow Phenomena. CISM Center, Udine, Italy.
Burns, J.R., Ramshaw, C., 2001. The intensification of rapid reactions in multiphase systems using slug flow in capillaries. Lab Chip 1, 10–15.
Celata, G.P., Cumo, M., Farello, G.E., Mariani, A., 1991. Flow pattern recognition in heated vertical channels: steady and transient conditions. Exp. Thermal Fluid Sci. 4, 737–746.
Chakrabarti, D.P., Das, G., Das, P.K., 2006. The transition from water continuous to oil continuous flow pattern. AIChE J. 52, 3668–3678.
Chakrabarti, D.P., Das, G., Das, P.K., 2007. Identification of stratified liquid–liquid flow through horizontal pipes by a non-intrusive optical probe. Chem. Eng. Sci. 62, 1861–1876.
Charoensombut-Amon, T., Martin, R.J., Kobayashi, R., 1986. Application of a generalized multiproperty apparatus to measure phase equilibrium and vapor phase densities of supercritical carbon dioxide in *n*-hexadecane system up to 26 MPa. Fluid Phase Equilibria 31, 89–104.
Chen, I.Y., Downing, R.S., Parish, R., Keshock, E., 1988. A reduced gravity flight experiment: observed flow regimes and pressure drops of vapor and liquid flow in adiabatic piping. In: AIChE Symposium Series 84 (263, Heat Transfer - Houston 1988), pp. 203–216.
D'Souza, R., Patrick, J.R., Teja, A.S., 1988. High pressure phase equilibria in the carbon dioxide–*n*-hexadecane and carbon dioxide–water systems. Can. J. Chem. Eng. 66, 319–323.
Durst, F., Ray, S., Ünsal, B., Bayoumi, O.A., 2005. The development lengths of laminar pipe and channel flows. Trans. ASME 127, 1154–1160.
Fairuzov, Y.V., Arenas-Medina, P., Verdejo-Fierro, J., Gonzalez-Islas, R., 2000. Flow pattern transitions in horizontal pipelines carrying oil–water mixtures: full-scale experiments. J. Energy Resour. Technol. 122, 169–176.
Farrar, B., Bruun, H.H., 1996. A computer based hot-film technique used for flow measurements in a vertical kerosene–water pipe flow. Int. J. Multiphase Flow 22, 733–751.
Hamad, F.A., Imberton, F., Bruun, H.H., 1997. An optical probe for measurements in liquid–liquid two-phase flow. Meas. Sci. Technol. 8, 1122–1132.
Hamad, F.A., Pierscionek, B.K., Bruun, H.H., 2000. A dual optical probe for volume fraction, drop velocity and drop size measurements in liquid–liquid two-phase flow. Meas. Sci. Technol. 11, 1307–1318.
Hernández, L., Juliá, J.E., Chiva, S., Paranjape, S., Ishii, M., 2006. Fast classification of two-phase flow regimes based on conductivity signals and artificial neural networks. Meas. Sci. Technol. 17, 1511–1521.
Hewitt, G.F., 1997. From gas–liquid to liquid–liquid two phase flow: a difficult journey. In: International Symposium on Liquid–Liquid Two-Phase Flow and Transport Phenomena, Antalya, Turkey, Nov. 3–7, 3–19.
Hu, B., Matar, O.K., Hewitt, G.F., Angeli, P., 2007. Mean and turbulent fluctuating velocities in oil–water vertical dispersed flows. Chem. Eng. Sci. 62, 1199–1214.
Hwang, J.J., Tseng, F.G., Pan, C., 2005. Ethanol–CO_2 two-phase flow in diverging and converging microchannels. Int. J. Multiphase Flow 31, 548–570.
Ioannou, K., Nydal, O.J., Angeli, P., 2005. Phase inversion in dispersed liquid–liquid flows. Exp. Thermal Fluid Sci. 29, 331–339.
Jana, A.K., Das, G., Das, P.K., 2006a. Flow regime identification of two-phase liquid–liquid upflow through vertical pipe. Chem. Eng. Sci. 61, 1500–1515.
Jana, A.K., Das, G., Das, P.K., 2006b. A novel technique to identify flow patterns during liquid–liquid two-phase upflow through a vertical pipe. Indust. Eng. Chem. Res. 45, 2381–2393.
Jana, A.K., Mandal, T.K., Chakrabarti, D.P., Das, G., Das, P.K., 2007. An optical probe for liquid–liquid two-phase flows. Meas. Sci. Technol. 18, 1563–1575.
Kashid, M.N., Agar, D.W., 2007. Hydrodynamics of liquid–liquid slug flow capillary microreactor: flow regimes, slug size and pressure drop. Chem. Eng. J. 131, 1–13.
Lin, R., 2008. Flow patterns of *n*-hexadecane–carbon dioxide liquid–liquid two-phase flow in vertical pipes of small diameter under high pressures. Master Thesis, Syracuse University, Syracuse, NY, USA.
Lin, S., Kew, P.A., 2001. Pressure fluctuation and flow regimes of air–water flow in a small tube. Exp. Heat Transfer 14, 135–144.

Lin, S., Kew, P.A., Cornwell, K., 1999. Characteristics of air/water flow in small tubes. Heat Technol. (Pisa) 17, 63–70.
Liu, H., Vandu, C.O., Krishna, R., 2005. Hydrodynamics of Taylor flow in vertical capillaries: flow regimes, bubble rise velocity, liquid slug length, and pressure drop. Ind. Eng. Chem. Res. 44, 4884–4897.
Lum, J.Y.-L., Al-Wahaibi, T., Angeli, P., 2006. Upward and downward inclined oil–water flows. Int. J. Multiphase Flow 32, 413–435.
Mandal, T.K., Chakrabarti, D.P., Gas, G., 2007. Oil–water flow through different diameter pipes - similarities and differences. Trans. IChemE A 85, 1123–1128.
Matthews, M.A., Rodden, J.B., Akgerman, A., 1987. High-temperature diffusion, viscosity, and density measurements in *n*-hexadecane. J. Chem. Eng. Data 32, 317–319.
Merkisz, J., Kozak, W., Bajerlein, M., Markowski, J., 2007. The influence of exhaust gases dissolved in diesel oil on fuel spray particulary parameters. SAE Paper 2007-01-0488.
Nädler, M., Mewes, D., 1997. Flow induced emulsification in the flow of two immiscible liquids in horizontal pipes. Int. J. Multiphase Flow 23, 53–68.
NIST, 2003. Thermophysical Properties of Hydrocarbon Mixtures Database (SUPERTRAPP), SRD 4, Version 3.1, Natl. Inst. Stand. Technol., Gaithersburg, MD.
Omebere-Iyari, N.K., Azzopardi, B.J., Ladam, L., 2007. Two-phase flow patterns in large diameter vertical pipes at high pressures. AIChE J. 53, 2493–2504.
Pawloski, J.L., Ching, C.Y., Shoukri, M., 2004. Measurement of void fraction and pressure drop of air–oil two-phase flow in horizontal pipes. J. Eng. Gas Turbines Power 126, 107–118.
Piela, K., Delfos, R., Ooms, G., Westerweel, J., Oliemans, R.V.A., Mudde, R.F., 2006. Experimental investigation of phase inversion in an oil–water flow through a horizontal pipe loop. Int. J. Multiphase Flow 32, 1087–1099.
Poling, B.E., Prausnitz, J.M., O'Connell, J.P., 2000. The properties of gases and liquids, fifth ed. McGraw-Hill.
Polishuk, I., Wisniak, J., Segura, H., 2003. Simultaneous prediction of the critical and sub-critical phase behavior in mixtures using equations of state II: carbon dioxide–heavy *n*-alkanes. Chem. Eng. Sci. 58, 2529–2550.
Raj, T.S., Chakrabarti, D.P., Das, G., 2005. Liquid–liquid stratified flow through horizontal conduits. Chem. Eng. Technol. 28, 899–907.
Rodriguez, O.M.H., Bannwart, A.C., 2006. Experimental study on interfacial waves in vertical core flow. J. Petroleum Sci. Eng. 54, 140–148.
Rodriguez, O.M.H., Oliemans, R.V.A., 2006. Experimental study on oil–water flow in horizontal and slightly inclined pipes. Int. J. Multiphase Flow 32, 323–343.
Satitchaicharoen, P., Wongwises, S., 2004. Two-phase flow pattern maps for vertical upward gas–liquid flow in mini-gap channels. Int. J. Multiphase Flow 30, 225–236.
Scheidgen, A., 1997. Fluid phase equilibria in binary and ternary mixtures of carbon dioxide with low-volatile organic substances up to 100 MPa (in German), Ph.D. Dissertation, Bochum: Ruhr-UniversitTat Bochum.
Schwarz, H.J., Prausnitz, J.M., 1987. Solubilities of methane, ethane, and carbon dioxide in heavy fossil-fuel fractions. Ind. Eng. Chem. Res. 26., 2360–2366.
Sebastian, H.M., Simnick, J.J., Lin, H., Chao, K., 1980. Vapor–liquid equilibrium in binary mixtures of carbon dioxide + *n*-decane and carbon dioxide + *n*-hexadecane. J. Chem. Eng. Data 25, 138–140.
Seleghim, P., Hervieu, E., 1998. Direct imaging of two-phase flows by electrical impedance measurements. Meas. Sci. Technol. 9, 1492–1500.
Shi, H., Cai, J., Jepson, W.P., 2001. Oil–water two-phase flows in large-diameter pipelines. J. Energy Resour. Technol. 123, 270–276.
Span, S., Wagner, W., 1996. A new equation of state for carbon dioxide covering the fluid region from the triple-point temperature to 1100 K at pressures up to 800 MPa. J. Phys. Chem. Ref. Data 25, 1509–1596.
Tanaka, H., Yamaki, Y., Kato, M., 1993. Solubility of carbon dioxide in pentadecane, hexadecane, and pentadecane + hexadecane. J. Chem. Eng. Data 38, 386–388.
Tavlarides, L.L., Anitescu, G., 2006. Supercritical diesel fuel composition, combustion process, and fuel system. US Patent Pub. No. 20060107586.
Tokeshi, M., Minagawa, T., Uchiyama, K., Hibara, A., Sato, K., Hisamoto, H., Kitamori, T., 2002. Continuous-flow chemical processing on a microchip by combining microunit operations and a multiphase flow network. Anal. Chem. 74, 1565–1571.
Trallero, J.L., Sarica, C., Brill, J.P., 1997. A study of oil/water flow patterns in horizontal pipes. SPE Prod. Facilities 12, 165–172.
Ujang, P.M., Lawrence, C.J., Hale, C.P., Hewitt, G.F., 2006. Slug initiation and evolution in two-phase horizontal flow. Int. J. Multiphase Flow 32, 527–552.
Virnau, P., Müller, M., MacDowell, L.G., Binder, K., 2004. Phase behavior of *n*-alkanes in supercritical solution: a Monte Carlo study. J. Chem. Phys. 121, 2169–2179.
Wegmann, A., von Rohr, P.R., 2006. Two phase liquid–liquid flows in pipes of small diameters. Int. J. Multiphase Flow 32, 1017–1028.
Wong, T.N., Yau, Y.K., 1997. Flow patterns in two-phase air–water flow. Int. Commun. Heat Mass Transfer 24, 111–118.
Wongwises, S., Pipathattakul, M., 2006. Flow pattern, pressure drop and void fraction of two-phase gas–liquid flow in an inclined narrow annular channel. Exp. Thermal Fluid Sci. 30, 345–354.
Zhao, D., Guo, L., Hu, X., Zhang, X., Wang, X., 2006. Experimental study on local characteristics of oil–water dispersed flow in a vertical pipe. Int. J. Multiphase Flow 32, 1254–1268.